Energy-efficient Connected Cruise Control with Lean Penetration of Connected Vehicles

Minghao Shen, *Graduate Student Member, IEEE,* Chaozhe R. He, *Member, IEEE*, Tamas G. Molnar, *Member, IEEE*, A. Harvey Bell, and Gábor Orosz, *Senior Member, IEEE*

***Abstract*—This paper focuses on energy-efficient longitudinal controller design for a connected automated truck that travels in mixed traffic consisting of connected and non-connected vehicles. The truck has access to information about connected vehicles beyond line of sight using vehicle-to-everything (V2X) communication. A novel connected cruise control design is proposed which incorporates additional delays into the control law when responding to distant connected vehicles to account for the finite propagation speed of traffic waves. The speeds of non-connected vehicles are modeled as stochastic processes. A fundamental theorem is proven which links the spectral properties of the motion signals to the average energy consumption. Controller synthesis for gain parameters is conducted over downstream traffic data and evaluated over a combination of synthetic and real cycles. It is demonstrated that even with lean penetration of connected vehicles, our controller can bring significant energy savings.**

***Index Terms*—Connected and Automated Vehicles, Eco-driving**

I. Introduction

ENERGY saving is an everlasting theme for the truck industry, since it has the potential to provide great financial and environmental benefits to the industry and the society. Vehicle automation and connectivity technologies may bring new opportunities for energy saving. On one hand, automated vehicles can be designed such that their controllers are carefully calibrated for energy efficiency. This includes longitudinal control systems such as adaptive cruise control (ACC) [1] and predictive cruise control where the speed profile is optimized according to the road elevation [2], [3], [4]. On the other hand, vehicle-to-everything (V2X) communication facilitates information sharing and cooperation between vehicles. This can be categorized into status-sharing, intent-sharing, agreement-seeking and prescriptive cooperation [5]. A popular approach to utilize cooperation in control is cooperative adaptive cruise control (CACC) [6], [7], [8], [9], [10], [11], [12] in which a platoon of connected automated vehicles is controlled to achieve great energy benefits. However, this requires all the vehicles involved to be connected and automated, which is not achievable in the near future.

In the forthcoming decades, researchers and engineers will need to deal with mixed traffic where vehicles may have various levels of connectivity and automation. The potential energy impact of connected vehicles in mixed traffic has attracted increasing attention in the recent years [13]. Various scenarios have been investigated, including highways [1], [14], [15], intersections [16] and roundabouts [17], while other studies have focused on the energy impact of the penetration rate of connected and automated vehicles [16], [18], [19].

In this paper, we design a connected cruise controller (CCC) [20] to control the longitudinal dynamics of a connected automated truck (CAT) traveling in mixed traffic which consists of connected and non-connected vehicles. We do not require the other vehicles to be automated, and only assume lean penetration of connectivity. We consider the lowest level of cooperation with other connected vehicles, i.e., status-sharing cooperation, where the CAT obtains the position and speed of vehicles ahead via V2X communication. We show that even a single connected vehicle in the downstream traffic can provide significant energy benefits for the CAT. This gives incentive to early adoptions of connectivity technologies.

In mixed traffic, with lean penetration of connectivity and low-level cooperation, a key challenge is to acquire information about surrounding traffic with high confidence for use in control. The CAT may be connected to vehicles in the far distance only, while surrounding non-connected vehicles may exhibit a large variety of different motions. Besides, a controller that ensures high energy efficiency for one motion profile may perform poorly for another.

A popular control approach is to first predict the motion of preceding vehicles, then optimize motion of the ego vehicle accordingly [21], [22]. While long accurate predictions can lead to large energy savings [23], such predictions are hard to acquire. As uncertainties grow with the prediction horizon, selected optimal actions could suffer large performance degradation. With V2X technology, beyond-line-of-sight information [24] can potentially improve the prediction accuracy, although the predict-then-optimize approach may still suffer from performance variations if the penetration of connected vehicles is lean. In what follows, instead of pursuing more precise prediction of transient human behavior, we minimize the energy consumption in the average sense based on vehicle trajectory data. We integrate data-driven methods and classical traffic models to optimize the energy efficiency of CCC.

This research was supported by the University of Michigan's Center for Connected and Automated Transportation through the US DOT grant 69A3551747105.

M. Shen, A. H. Bell, and G. Orosz are with the Department of Mechanical Engineering, University of Michigan, Ann Arbor, MI 48109, USA (e-mail: mhshen@umich.edu, ahbelliv@umich.edu, orosz@umich.edu).

C. R. He is with PlusAI Inc., Cupertino, CA 95014, USA (email: hchaozhe@umich.edu).

T. G. Molnar is with the Department of Mechanical and Civil Engineering, California Institute of Technology, Pasadena, CA 91125, USA (email: tmolnar@caltech.edu).

G. Orosz is also with the Department of Civil and Environmental Engineering, University of Michigan, Ann Arbor, MI 48109, USA.

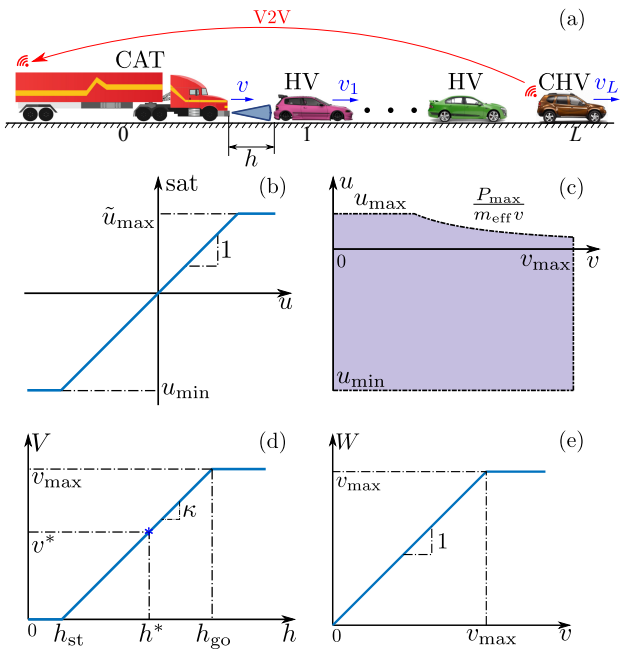

Fig. 1. (a) A connected automated truck (CAT) driving in mixed traffic that consists of connected human-driven vehicles (CHVs) and non-connected human-driven vehicles (HVs). (b,c) Saturation function. (d) Range policy. (e) Speed policy.

In this paper, we propose an energy-efficient longitudinal control strategy for CATs by utilizing data from V2X connectivity. This is achieved by three contributions. First, we propose a novel CCC design for the CAT, which accounts for the fact that connected vehicles may travel far ahead of the CAT, hence it may not be optimal to respond to their motions immediately. Thus, an additional delay is incorporated into the response to the motion of distant vehicles [25] allowing the CAT to "wait" for velocity fluctuations to propagate. Second, we propose a stochastic modeling framework to capture the longitudinal motions of human-driven vehicles preceding the CAT. We estimate the spectral properties of their motions from V2X data [26], and we state and prove a fundamental theorem to establish the relationship between the spectral properties and the average energy consumption of the CAT. Third, we use this theorem to formulate a V2X data-driven optimization problem, that tunes the controller gains and additional delays to maximize the CAT's energy efficiency. The optimality of the controller parameters is validated statistically using large amount of synthetic data as well as experimental data.

The remainder of this paper is organized as follows. In Section II, we model the dynamics of the CAT, formulate a connected cruise controller using delayed V2X information, and highlight the parameters to be optimized. In Section III, we include necessary mathematical background on stochastic modeling. In Section IV, we model the motion of preceding vehicles as stochastic processes, and establish the optimization problem which enables us to find the energy-optimal controller parameters. In Section V, we validate the optimality in terms of energy consumption based on large amount of simulations. Section VI concludes the paper and discusses future directions.

II. Connected Cruise Control Design

In this section, we design a longitudinal controller for a connected and automated truck (CAT) that drives in mixed traffic consisting of connected human-driven vehicles (CHVs) and non-connected human-driven vehicles (HVs); see Fig. 1(a). The truck can measure its own speed v, the distance headway h and the speed v_1 of the vehicle immediately ahead using range sensors such as camera, LiDAR or radar. In this work, we assume no elevation along the road and no headwind. We remark, however, that road elevation can be significant to energy consumption, but it is beyond the scope of this paper. We formulate the longitudinal dynamics of the truck as

$$\begin{aligned} \dot{h}(t) &= v_1(t) - v(t)\,, \\ \dot{v}(t) &= -\frac{1}{m_{\text{eff}}}\left(mg\xi + kv^2(t)\right) + \frac{T_{\text{w}}(t)}{m_{\text{eff}}R}\,. \end{aligned} \tag{1}$$

Here the dot refers to differentiation with respect to time t. The effective mass $m_{\text{eff}} = m + I/R^2$ consists of the mass m of the truck and the mass moment of inertia I of its rotating elements. The radius of the wheels is denoted by R, g is the gravitational constant, ξ denotes the rolling resistance coefficient, and k is the air drag coefficient incorporating air density and the vehicle's frontal area. In this paper, we choose $m = 29484$ [kg], $I = 39.9$ [kg m^2], $R = 0.504$ [m], $\xi = 0.006$, $k = 3.84$ [kg/m] [2]. We describe the nonlinear physical effects by the function

$$f(v) = \frac{1}{m_{\text{eff}}}\left(mg\xi + kv^2\right)\,. \tag{2}$$

To control the longitudinal motion of the truck, the wheel torque T_{w} is generated to achieve desired acceleration. When $T_{\text{w}} > 0$, the torque is provided by the powertrain, while when $T_{\text{w}} < 0$ the torque comes from the braking system. The control input u is considered to be the commanded longitudinal acceleration. The effect of the control input is subject to a time delay and saturation:

$$\frac{T_{\text{w}}(t)}{m_{\text{eff}}R} = \text{sat}\big(u(t-\sigma)\big)\,, \tag{3}$$

where σ models the delay in the powertrain system and the saturation function is given by

$$\text{sat}(u) = \begin{cases} u_{\min} & \text{if} \quad u \le u_{\min}\,, \\ u & \text{if} \quad u_{\min} < u < \tilde{u}_{\max}\,, \\ \tilde{u}_{\max} & \text{if} \quad u \ge \tilde{u}_{\max}\,, \end{cases} \tag{4}$$

and

$$\tilde{u}_{\max} = \min\left\{u_{\max}, \frac{P_{\max}}{m_{\text{eff}}v}\right\}\,. \tag{5}$$

The saturation results from the limited available engine torque (associated with $u_{\max}$), engine power $P_{\max}$ and braking torque (associated with $u_{\min}$). They are illustrated in Fig. 1(b,c). Here we consider the parameters $u_{\min} = -6$ [m/s^2], $u_{\max} = 2$ [m/s^2], $P_{\max} = 300.65$ [kW], $m_{\text{eff}} = 29641$ [kg]; see [23].

Considering the nonlinear physical effects $f(v)$, the controller consists of two terms

$$u(t) = \tilde{f}\big(v(t)\big) + a_{\text{d}}(t)\,, \tag{6}$$

where compensation term $\tilde{f}(v)$ is implemented by a lower-level controller in order to cancel the resistance term $f(v)$, while $a_{\rm d}$ defines the desired acceleration given by a higher-level controller that is to be designed.

With on-board range sensors such as radar or LiDAR, the truck can detect the headway and the speed of the preceding vehicle. This enables *adaptive cruise control (ACC)* with

$$a_{\rm d} = \alpha\,(V(h) - v) + \beta\,(W(v_1) - v)\,. \tag{7}$$

This control law is constructed according to the optimal velocity model (OVM) [27], [28] that describes human car-following behavior. The first term aims to maintain a desirable headway h, and the second term aims to match the speed v of the ego truck to the speed v_1 of the preceding vehicle.

The nonlinear functions V and W in (7) are the range policy and the speed policy, respectively. The range policy

$$V(h) = \max\left\{0, \min\{\kappa(h - h_{\rm st}), v_{\max}\}\right\}, \tag{8}$$

shown in Fig. 1(d), is the desired speed as a function of the headway. When the headway is small, the truck intends to stop, while when the headway is large, it aims to travel at maximum speed $v_{\max}$. For headways in between, the desired speed increases linearly with gradient $\kappa = v_{\max}/(h_{\rm go} - h_{\rm st})$. Apart from the piecewise linear range policy (8), there exist many other possible choices such as arctangent function [29] or quadratic spacing policies [30]. The speed policy

$$W(v) = \min\{v, v_{\max}\}\,, \tag{9}$$

shown in Fig. 1(e), is designed to keep the speed of truck under the speed limit $v_{\max}$ when preceding vehicles are speeding. In this paper, we set $v_{\max} = 35$ [m/s], $h_{\rm st} = 5$ [m], $h_{\rm go} = 63.33$ [m], yielding $\kappa = 0.6$ [1/s].

With vehicle-to-everything (V2X) communication, the truck has access to information about preceding vehicles, including their position and speed. In this paper, we establish energy-efficient longitudinal controllers by leveraging the information from V2X connectivity in the case of lean (very low) penetration of connected vehicles. Specifically, we focus on the scenario in Fig. 1(a) where only a single vehicle (with index L) is connected to the CAT in the downstream traffic.

Let $\mathcal{I}$ denote the indices of the vehicles whose information the CAT has access to. This includes the vehicle immediately ahead of the truck, which is monitored by the range sensors, as well as the CHVs who share their motion information via V2X connectivity. For example, in Fig. 1(a) the CAT has access to information about vehicles indexed 1 and L, i.e., $\mathcal{I} = \{1, L\}$. Then, the CAT may respond to multiple preceding vehicles by using *connected cruise control (CCC)* [31] with

$$a_{\rm d} = \alpha\,(V(h) - v) + \sum_{i\in\mathcal{I}} \beta_i\,(W(v_i) - v)\,. \tag{10}$$

This control law is an extension of the ACC strategy in (7), where the second term matches the speed v of the ego truck with both the speed v_1 of the vehicle immediately ahead and the speeds of the connected vehicles in the distance.

Through V2X communication, the truck can potentially connect to vehicles a few hundred meters in the distance. The behavior of vehicles far ahead may not immediately influence the behavior of vehicles surrounding the truck, instead, the effects may occur a few seconds later as traffic waves propagate with a finite speed along vehicle chains [32], [33]. This phenomenon is captured by many traffic flow models such as the Lighthill-Whitham-Richards model [34], [33] or Newell's equation [35]. Thus, the truck can intentionally *wait* before responding to vehicles far in the distance. Using this idea, we propose a *CCC design with additional delay* (CCC-Delay):

$$a_{\rm d}(t) = \alpha\big(V(h(t)) - v(t)\big) + \sum_{i\in\mathcal{I}} \beta_i\big(W(v_i(t-\sigma_i)) - v(t)\big). \tag{11}$$

The key novelty of the proposed controller (11) is the introduction of the time delay (waiting time) σ_i as design parameter. While delays often cause instability or reduce control performance, this additional delay will be shown to improve the energy efficiency of the CAT by accounting for the propagation time of traffic waves.

The most fundamental requirement for the controller (11) is to realize stable motion for the CAT. In order to analyze the stability of the closed-loop system defined by (1,6,11), we linearize the system around the equilibrium

$$h(t) \equiv h^*\,, \quad v(t) = v_i(t) \equiv v^* = V(h^*)\,, \tag{12}$$

for $i \in \mathcal{I}$. Defining the headway and speed perturbations $\tilde{h} = h - h^*$, $\tilde{v} = v - v^*$, $\tilde{v}_i = v_i - v^*$, we may obtain the linearized dynamics in the form

$$\begin{aligned}\dot{\tilde{h}}(t) &= \tilde{v}_1(t) - \tilde{v}(t)\,,\\ \dot{\tilde{v}}(t) &= \alpha\big(\kappa\tilde{h}(t-\sigma) - \tilde{v}(t-\sigma)\big)\\ &\quad + \sum_{i\in\mathcal{I}} \beta_i\big(\tilde{v}_i(t-(\sigma+\sigma_i)) - \tilde{v}(t-\sigma)\big)\,.\end{aligned} \tag{13}$$

For analysis in frequency domain, we apply the Laplace transform with zero initial condition, which leads to

$$V(s) = \sum_{i\in\mathcal{I}} T_i(s) V_i(s)\,. \tag{14}$$

Here $V(s)$ and $V_i(s)$ denote the Laplace transforms of the speed perturbation $\tilde{v}(t)$ of the CAT and the speed perturbations $\tilde{v}_i(t)$ of the preceding vehicles, while the link transfer functions are defined as

$$T_1(s) = \frac{\beta_1 s + \alpha\kappa}{\mathcal{D}(s)}\,, \quad T_i(s) = \frac{\beta_i s e^{-s\sigma_i}}{\mathcal{D}(s)}\,, \tag{15}$$

for $i \in \mathcal{I} \setminus \{1\}$, where

$$\mathcal{D}(s) = s^2 e^{s\sigma} + \left(\alpha + \sum_{i\in\mathcal{I}} \beta_i\right) s + \alpha\kappa \tag{16}$$

gives the characteristic function.

In order to ensure that the truck is able to approach the equilibrium (12), the linearized system (13) needs to be plant stable [31]. That is, all roots of the characteristic equation $\mathcal{D}(s) = 0$ must have negative real parts. This is satisfied when the parameters $(\alpha, \beta_i), i \in \mathcal{I}$ are selected from the region

$$\begin{aligned}&\alpha > 0\,,\\ &\underline{\omega}\sin(\underline{\omega}\sigma) - \alpha < \sum_{i\in\mathcal{I}} \beta_i < \overline{\omega}\sin(\overline{\omega}\sigma) - \alpha\,,\end{aligned} \tag{17}$$

where $\underline{\omega}$ and $\overline{\omega}$ are the solutions of the transcendental equation $\alpha\kappa = \omega^2\cos(\omega\sigma)$ such that $0 < \underline{\omega} < \overline{\omega} < \frac{\pi}{2}$. Note that the additional delay σ_i does not influence the plant stability of the closed-loop system [25].

To evaluate the tank-to-distance energy consumption [36] of the CAT, we use the energy consumption per unit mass over the time interval $t \in [t_0, t_\mathrm{f}]$ as metrics:

$$w = \int_{t_0}^{t_\mathrm{f}} v(t) g\big(\dot{v}(t) + f(v(t))\big)\mathrm{d}t\,, \tag{18}$$

where g depends on the engine and powertrain type. Here, we consider trucks with internal combustion engines and use $g(x) = \max\{x, 0\}$, so that energy is assumed to be consumed only when $u > 0$. For hybrid electric vehicles or electric vehicles, one may choose different expression for g [37]. Our goal is to find the controller parameters $(\alpha, \beta_i, \sigma_i), i \in \mathcal{I}$ that minimize w while also ensuring plant stability.

III. Stochastic Modeling

In this section, we propose a stochastic approach where we model the motion of the preceding vehicles using stochastic processes. For simplicity, we limit our analysis to a specific family of stochastic processes, Gaussian processes, which result in physically realistic vehicle motions.

Consider a closed-loop system with dynamics (1,6,11) where the inputs $v_i, i \in \mathcal{I}$ are described by stochastic processes. The goal is to relate the gain parameters $(\alpha, \beta_i), i \in \mathcal{I}$ and the delays $\sigma_i, i \in \mathcal{I}$ through the system output v to the energy consumption w defined in (18). To simplify the analysis, we make three assumptions about the input processes $v_i, i \in \mathcal{I}$: (i) they are wide-sense stationary (WSS); (ii) they are differentiable; (iii) they are Gaussian processes. We discuss these assumptions more rigorously below and relate them to spectral theory.

The stationarity assumption enables us to apply spectral analysis, and link the controller parameters to the characteristics of the output process v. To achieve this, we need a few definitions.

Definition 1 (Strict-sense Stationary (SSS))**.** A stochastic process $\{X_t\}_{t\in T}$ is *strict-sense stationary* if for any indices $t_1, \cdots, t_k \in T$ and sets $A_1, \cdots, A_k$, the probabilities

$$\mathbb{P}(X_{t_1+t} \in A_1, \cdots, X_{t_k+t} \in A_k)\,, \tag{19}$$

do not depend on t, where $t \in T$.

Specifically, choosing $t_1 = 0$ and $k = 1$, shows that the marginal distribution of random variable X_t is time-invariant. In general, SSS is a strong requirement which is hard to satisfy. However, in many cases, the first and second moments of the distribution can provide enough information. Thus, many theories, such as spectral analysis, only require wide-sense stationarity, where stationarity is enforced only on first and second moments.

Definition 2 (Mean and Correlations)**.** For a stochastic process $\{X_t\}_{t\in T}$, the *mean* and the *autocorrelation* are given by

$$\mu_X(t) = \mathbb{E}[X_t]\,, \quad R_{XX}(s,t) = \mathbb{E}[X_s X_t]\,, \tag{20}$$

where $\mathbb{E}[\cdot]$ denotes the expected value. Considering another stochastic process $\{Y_t\}_{t\in T}$ defined on the same probability space, we define the *cross-correlation* as

$$R_{XY}(s,t) = \mathbb{E}[X_s Y_t]\,. \tag{21}$$

Definition 3 (Wide-sense Stationary (WSS))**.** A stochastic process $\{X_t\}_{t\in T}$ is called wide-sense stationary if there exist a constant m and a function $r(t)$, $t \in T$, such that

$$\mu_X(t) \equiv m\,, \quad R_{XX}(s,t) = r(t-s)\,, \quad \forall s, t \in T\,. \tag{22}$$

That is, when $\{X_t\}_{t\in T}$ is WSS, $R_{XX}(s,t)$ is a function of $(t-s)$ and we can write $R_{XX}(\tau) = R_{XX}(t-s)$ without ambiguity. One may verify that autocorrelation is symmetric, that is, $R_{XX}(s,t) = R_{XX}(t,s)$ for a general stochastic process, yielding $R_{XX}(\tau) = R_{XX}(-\tau)$ for a WSS process. Similarly, the cross-correlation is also symmetric. Also note that the autocorrelation $R_{XX}(0)$ gives the second moments; cf. (20). We assume that speed perturbations of the preceding vehicles $\tilde{v}_i$ are WSS, that is, $v_i = v^* + \tilde{v}_i$ where v^* denotes the equilibrium speed and $\mu_{\tilde{v}_i} = 0$, for all $i \in \mathcal{I}$.

For a signal that satisfies WSS condition, we can apply spectral analysis and determine the input/output relationship for linear time-invariant (LTI) systems. Such analysis utilizes the power spectral density which can be defined via the continuous-time Fourier transform of the WSS process.

Definition 4 (Power spectral density [38])**.** For a WSS process X_t, the *power spectral density* is the Fourier transform of the autocorrelation function:

$$S_{XX}(\omega) = \mathcal{F}[R_{XX}(\tau)] = \int_{-\infty}^{\infty} R_{XX}(\tau) e^{-\mathrm{j}\omega\tau}\mathrm{d}\tau\,, \tag{23}$$

where ω denotes the angular frequency.

Since $R_{XX}(\tau) = R_{XX}(-\tau)$, the power spectral density $S_{XX}(\omega)$ is a non-negative real number and one can also show that $S_{XX}(\omega) = S_{XX}(-\omega)$. For LTI systems with input being a WSS process, the power spectral density of the output process can be calculated using the following lemma [38].

Lemma 1 (Spectral Analysis of LTI Systems)**.** *For a linear time invariant system with transfer function $G(s)$, if the input signal X_t is a WSS process, then the output signal Y_t is also WSS. The first and second moments of Y_t are given by*

$$\mu_Y = G(0)\mu_X\,, \quad S_{YY}(\omega) = |G(\mathrm{j}\omega)|^2 S_{XX}(\omega)\,. \tag{24}$$

The proof can be found in Chapter 8.2 of [38].

Similarly, the *cross power spectral density* can be defined as the Fourier transform of the cross-correlation function

$$S_{XY}(\omega) = \mathcal{F}[R_{XY}(\tau)]\,, \tag{25}$$

which may be a complex number. The following lemma defines the input/output relationship of signals passing through different LTI systems [38].

Lemma 2. *Given two signals X_t and Y_t separately passing through two LTI systems with transfer functions $G_1(s)$ and $G_2(s)$, respectively, the cross power spectral density of the corresponding outputs Z_t and P_t is*

$$S_{ZP}(\omega) = G_1(\mathrm{j}\omega)G_2^*(\mathrm{j}\omega)S_{XY}(\omega)\,, \tag{26}$$

where star denotes complex conjugate.

The proof can be found in Chapter 8.2 of [38].

In practice, it is reasonable to assume that the speeds of preceding vehicles are continuously differentiable, i.e., accelerations are continuous. Specifically, for a WSS process X_t, the time derivative $\dot{X}_t$ has the following properties:

(a) X_t and $\dot{X}_t$ are jointly WSS
(b) $\mu_{\dot{X}}(t) = 0$
(c) $R_{\dot{X}X}(\tau) = \frac{\mathrm{d}}{\mathrm{d}\tau} R_{XX}(\tau) = -R_{X\dot{X}}(\tau)$
(d) $R_{\dot{X}X}(0) = R_{X\dot{X}}(0) = 0$
(e) $R_{\dot{X}\dot{X}}(\tau) = -\frac{\mathrm{d}^2}{\mathrm{d}\tau^2} R_{XX}(\tau)$

The proof can be found in Chapter 7.2 of [38].

Apart from being differentiable, the speeds of preceding vehicles are assumed to be Gaussian processes. This simplifies the analysis and enables us to derive analytical results.

Definition 5 (Gaussian Process (GP))**.** A stochastic process $\{X_t\}_{t\in T}$ is a *Gaussian process* if for every finite set of indices $t_1, \cdots, t_k \in T$, $X(t_1, \cdots, t_k) = (X_{t_1}, \cdots, X_{t_k})$ is multivariate Gaussian random variable.

Gaussian process has the following nice properties [38].

(a) Gaussian process is uniquely determined by its mean function and autocorrelation function.
(b) If a Gaussian process is WSS, then it is SSS.
(c) For a linear system, if the input signal is a Gaussian process, then the output is also a Gaussian process.
(d) If a Gaussian process X_t is mean square differentiable, then $\dot{X}_t$ is also a Gaussian process.

In this section, we have established necessary properties of the motions of preceding vehicles by assuming them to be stationary differentiable Gaussian processes. We are now ready to apply spectral analysis on the closed-loop linearized system (13) to derive the distribution of the CAT's motion, as well as the average energy consumption. This allows us to optimize the controller parameters $(\alpha, \beta_i, \sigma_i), i \in \mathcal{I}$ for energy efficiency based on the data obtained from V2X connectivity.

IV. Data-driven Controller Optimization

In this section, we propose a method to determine the energy-optimal parameters for the proposed controller using traffic data. First we derive an optimization problem assuming oracle knowledge about the spectral density of the preceding vehicles' speed. Then we introduce two estimators for the cross power spectral density, and finally formalize the data-driven controller optimization method.

A. Optimization with Oracle Knowledge

Here we utilize the theory introduced in the previous section, to apply spectral analysis for the linearized system (13), derive analytical expression for the expectation of the energy consumption defined in (18), and formulate an optimization problem to determine energy-optimal controller parameters. We achieve these results under the following assumption.

Assumption 1. The inputs $\tilde{v}_i, i \in \mathcal{I}$ are WSS, mean-square differentiable Gaussian processes with zero mean.

For the linearized system (13), the nonlinear physical effects $f(v)$ and saturation $\mathrm{sat}(\cdot)$ are dismissed. Therefore, we consider the surrogate energy consumption model

$$\bar{w} = \int_{t_0}^{t_\mathrm{f}} v(t) g\big(\dot{v}(t)\big) \mathrm{d}t \,, \tag{27}$$

cf. (18). Then, the following theorem provides an analytical expression for the energy consumption.

Theorem 3. *Consider the linearized dynamics* (13) *around equilibrium* (12) *under Assumption 1. The expectation of the energy consumption defined in* (27) *is given by*

$$\mathbb{E}[\bar{w}] = (t_\mathrm{f} - t_0) \frac{v^*}{\sqrt{2\pi}} \vartheta \,, \tag{28}$$

where

$$\vartheta^2 = \frac{1}{\pi} \sum_{i,j\in\mathcal{I}} \int_0^\infty \omega^2 T_i(\mathrm{j}\omega) T_j^*(\mathrm{j}\omega) S_{\tilde{v}_i\tilde{v}_j}(\omega) \mathrm{d}\omega \tag{29}$$

represents the variance of $\dot{v}$, which is equal to the variance of $\dot{\tilde{v}}$.

Proof. Under Assumption 1, the output $\tilde{v}$ is a WSS Gaussian process with zero mean. According to (14), the output signal $\tilde{v}$ can be decomposed into response η_i to each input signal $\tilde{v}_i$:

$$\tilde{v}(t) = \sum_{i\in\mathcal{I}} \eta_i(t) \,. \tag{30}$$

In time domain, we have

$$\begin{aligned} R_{\tilde{v}\tilde{v}}(\tau) &= \mathbb{E}[\tilde{v}(t)\tilde{v}(t+\tau)] \\ &= \sum_{i,j\in\mathcal{I}} \mathbb{E}[\eta_i(t)\eta_j(t+\tau)] \\ &= \sum_{i,j\in\mathcal{I}} R_{\eta_i\eta_j}(\tau) \,. \end{aligned} \tag{31}$$

Taking the Fourier transform and noting that $\mathcal{F}[R_{\tilde{v}\tilde{v}}(\tau)] = S_{\tilde{v}\tilde{v}}(\omega)$ and $\mathcal{F}[R_{\tilde{\eta}_i\tilde{\eta}_j}] = S_{\tilde{\eta}_i\tilde{\eta}_j}(\omega)$, we obtain

$$\begin{aligned} S_{\tilde{v}\tilde{v}}(\omega) &= \sum_{i,j\in\mathcal{I}} S_{\eta_i\eta_j}(\omega) \\ &= \sum_{i,j\in\mathcal{I}} T_i(\mathrm{j}\omega) T_j^*(\mathrm{j}\omega) S_{\tilde{v}_i\tilde{v}_j}(\omega) \,, \end{aligned} \tag{32}$$

where in the last step we used Lemma 2. Note that when $i = j$, we have $S_{\eta_i\eta_j} = |T_{ij}(\mathrm{j}\omega)|^2 S_{\tilde{v}_i\tilde{v}_j}(\omega)$.

The speed perturbation of the truck $\tilde{v}$ as well as its derivative $\dot{\tilde{v}}$ are WSS Gaussian processes with zero mean. Let us consider the second moments

$$\varsigma^2 = R_{\tilde{v}\tilde{v}}(0) \,, \quad \vartheta^2 = R_{\dot{\tilde{v}}\dot{\tilde{v}}}(0) \,. \tag{33}$$

Since for WSS process $R_{\dot{X}\dot{X}}(\tau) = -\frac{\mathrm{d}^2}{\mathrm{d}\tau^2} R_{XX}(\tau)$, we can express the variance of $\dot{\tilde{v}}$ as

$$\begin{aligned} \vartheta^2 &= R_{\dot{\tilde{v}}\dot{\tilde{v}}}(0) \\ &= -\frac{\mathrm{d}^2}{\mathrm{d}\tau^2} R_{\tilde{v}\tilde{v}}(\tau)\Big|_{\tau=0} \\ &= \mathcal{F}^{-1}[\omega^2 S_{\tilde{v}\tilde{v}}(\omega)]|_{\tau=0} \\ &= \frac{1}{2\pi} \int_{-\infty}^{\infty} \omega^2 S_{\tilde{v}\tilde{v}}(\omega) e^{\mathrm{j}\omega\tau} \mathrm{d}\omega \Big|_{\tau=0} \,. \end{aligned} \tag{34}$$

Since $S_{\tilde{v}\tilde{v}}(\omega) = S_{\tilde{v}\tilde{v}}(-\omega)$, we have

$$\begin{aligned}\vartheta^2 &= \frac{1}{\pi}\int_0^\infty \omega^2 S_{\tilde{v}\tilde{v}}(\omega)\mathrm{d}\omega \\ &= \frac{1}{\pi}\sum_{i,j\in\mathcal{I}}\int_0^\infty \omega^2 T_i(\mathrm{j}\omega)T_j^*(\mathrm{j}\omega)S_{\tilde{v}_i\tilde{v}_j}(\omega)\mathrm{d}\omega.\end{aligned} \tag{35}$$

Thus, considering $R_{\tilde{v}\dot{\tilde{v}}}(0) = 0$, we can write down the joint distribution of $v = \tilde{v} + v^*$ and $\dot{v} = \dot{\tilde{v}}$ as follows

$$p(v,\dot{v}) = \frac{1}{2\pi\varsigma\vartheta}\exp\left(-\frac{(v-v^*)^2}{2\varsigma^2} - \frac{\dot{v}^2}{2\vartheta^2}\right). \tag{36}$$

From SSS assumption, the distributions of $v(t)$ and $\dot{v}(t)$ are time-invariant. The mean value of the energy consumption $\bar{w}$ defined in (27) can be calculated as

$$\begin{aligned}\mathbb{E}[\bar{w}] &= \int_{t_0}^{t_\mathrm{f}}\mathrm{d}t\int_{-\infty}^{\infty}\mathrm{d}v\int_{-\infty}^{\infty} v g(\dot{v})p(v,\dot{v})\mathrm{d}\dot{v} \\ &= (t_\mathrm{f}-t_0)\int_{-\infty}^{\infty}\mathrm{d}v\int_0^\infty v\dot{v}p(v,\dot{v})\mathrm{d}\dot{v} \\ &= (t_\mathrm{f}-t_0)\frac{1}{2\pi\varsigma\vartheta}\left[\int_{-\infty}^{\infty} v\exp\left(-\frac{(v-v^*)^2}{2\varsigma^2}\right)\mathrm{d}v\right] \\ &\qquad\times\left[\int_0^\infty \dot{v}\exp\left(-\frac{\dot{v}^2}{2\vartheta^2}\right)\mathrm{d}\dot{v}\right] \\ &= (t_\mathrm{f}-t_0)\frac{v^*}{\sqrt{2\pi}}\vartheta\,.\end{aligned} \tag{37}$$

This completes the proof. □

Theorem 3 provides a concise closed-form expression in (28) for the average energy consumption, which is proved to be proportional to the standard deviation ϑ of the ego truck's acceleration $\dot{v}$. The standard deviation ϑ is analytically calculated in (29) with the spectral theory introduced in Section III, based on the linearized closed-loop system (13) and the spectral density of the input signal $\tilde{v}_i$. As shown in (29), the standard deviation ϑ is related not only to the closed-loop transfer function $T_i(\mathrm{j}\omega)$ but also to the relationship among input signals given by $S_{ij}(\omega)$. Note that the traffic wave propagation phenomenon mentioned before can be captured by $S_{1L}(\omega)$, that is the cross spectral density associated with the speeds of vehicle L in the distance and vehicle 1 immediately in front of the ego truck.

As consequence of Theorem 3, parameters that minimize ϑ^2, the variance of $\dot{v}$, also minimize the average energy consumption. In this paper, we fix $\alpha = 0.4$ [1/s] for safety considerations [39], and search for the optimal parameters $(\beta_i, \sigma_i), i \in \mathcal{I}$. We find their values by solving an optimization problem summarized in the following corollary of Theorem 3. Note that the results can be easily extended to include α.

Corollary 3.1. *Consider the linearized dynamics* (13) *around equilibrium* (12) *under Assumption 1. The optimal values of the control parameters* $(\beta_i, \sigma_i), i \in \mathcal{I}$ *that minimize the expectation of the energy consumption* (27) *while maintaining plant stability can be found by solving the optimization problem*

$$\begin{aligned}\min_{(\beta_i,\sigma_i)} J &= \sum_{i,j\in\mathcal{I}}\int_0^\infty \omega^2 T_i(\mathrm{j}\omega)T_j^*(\mathrm{j}\omega)S_{\tilde{v}_i\tilde{v}_j}(\omega)\mathrm{d}\omega\ , \\ \text{s.t.}\quad &(\beta_i)\in\Omega\ ,\end{aligned} \tag{38}$$

where Ω *is the plant stable region defined in* (17).

Power spectral densities of speed perturbations of preceding vehicles are included in the objective function of (38) when $i = j$. Furthermore, the cross power spectral densities in the objective function capture the correlations between the speed perturbation signals of the preceding vehicles when $i \neq j$. Such correlations are especially significant in dense traffic where the motions of subsequent vehicles are typically strongly coupled. For example, Newell's car-following model considers the speed of a following vehicle as delayed copy of the vehicles ahead [35]. Computing the cross power spectral density allows us to capture and utilize such strong correlations to improve energy efficiency.

Remark. Theorem 3 relies on linear approximations of both the dynamics and the energy measure as opposed to directly considering nonlinear expressions. The advantage of the linear surrogate energy model (27) is that it leads to the average energy consumption in closed form, enabling the construction of the optimization problem (38). The linear approximation, however, may lead to suboptimal performance under nonlinear dynamics, which will be investigated via numerical results. We remark that there exist spectral analysis techniques for nonlinear stochastic systems [40], [41], although these can be very involved and are beyond the scope of this work.

B. Data-driven Optimization

In practice, the true value of the cross power spectral density $S_{\tilde{v}_i\tilde{v}_j}(\omega)$ is unknown. Instead, we need to estimate it from finite amount of data sampled in discrete time. In this paper, we utilize two estimators: periodogram and Welch's method [42].

Consider observation data of two velocity signals $\{v_i(t_k)\}_{k=0}^{N-1}$ and $\{v_j(t_k)\}_{k=0}^{N-1}$ for time instances $t_k = k\Delta t$. First, we subtract from each term their sample mean to get the centralized data $\{\tilde{v}_i(t_k)\}_{k=0}^{N-1}$ and $\{\tilde{v}_j(t_k)\}_{k=0}^{N-1}$. Let $\{\tilde{V}_i(\omega_k)\}_{k=0}^{N-1}$ and $\{\tilde{V}_j(\omega_k)\}_{k=0}^{N-1}$, $\omega_k = \frac{2\pi k}{N\Delta t}$ be the discrete-time Fourier transforms of $\{\tilde{v}_i(t_k)\}_{k=0}^{N-1}$ and $\{\tilde{v}_j(t_k)\}_{k=0}^{N-1}$, respectively. The periodogram method estimates the cross-spectral density with

$$\hat{S}_{\tilde{v}_i\tilde{v}_j}(\omega_k) = \frac{2\Delta t}{N}\tilde{V}_i(\omega_k)\tilde{V}_j^*(\omega_k)\,. \tag{39}$$

When $i = j$, it reduces to the one-sided estimator of power spectral density

$$\hat{S}_{\tilde{v}_i\tilde{v}_i}(\omega_k) = \frac{2\Delta t}{N}\left|\tilde{V}_i(\omega_k)\right|^2. \tag{40}$$

The periodogram estimator is asymptotically unbiased, but suffers from high variance. We can apply the following methods to reduce the variance. In time domain, we can split the original signals into segments, calculate the periodogram of each segment, then average them for each frequency. In frequency domain, we can apply window functions, such as Hamming window, and calculate the periodogram for windowed signals. Welch's method [43] combines the two solutions together. First we split each original signal into overlapping segments, with 50% overlap ratio. Then we apply window

function to each segment and calculate the periodogram for each windowed segment. Finally, we average over all the periodograms for each frequency. Welch's method can achieve lower variance, but at the cost of frequency resolution. We will see later in Section V-C that the variance reduction property can help us obtain better controller gains β_i, but the low resolution poses limitations on getting appropriate information delay σ_i.

It is straightforward to replace the power spectral density $S_{\tilde{v}_i\tilde{v}_j}$ in (38) with periodogram estimator, and rewrite the optimization problem for discrete-time observations:

$$\begin{aligned}\min_{(\beta_i,\sigma_i)} J &\approx \frac{2\Delta t}{N}\sum_{k=0}^{N-1}\sum_{i,j\in\mathcal{I}}\omega_k^2 T_i(\mathrm{j}\omega_k)T_j^*(\mathrm{j}\omega_k)\tilde{V}_i(\omega_k)\tilde{V}_j^*(\omega_k)\\ &= \frac{2\Delta t}{N}\sum_{k=0}^{N-1}\omega_k^2\left|\sum_{i\in\mathcal{I}}T_i(\mathrm{j}\omega_k)\tilde{V}_i(\omega_k)\right|^2\\ &= \frac{2\Delta t}{N}\sum_{k=0}^{N-1}\omega_k^2\left|\tilde{V}(\omega_k)\right|^2\\ &\text{s.t. } (\beta_i)\in\Omega.\end{aligned} \tag{41}$$

Note that the constraint $(\beta_i)\in\Omega$ is affine in β_i based on (17), while the cost is a complicated nonlinear function of (β_i,σ_i) due to the expression (15) of the transfer function $T_i(\mathrm{j}\omega)$. Therefore, the optimization problem (41) needs to be solved with a general nonlinear optimization solver. In this paper, we use `fmincon` [44] with interior-point method.

The optimization problem is similar for Welch's method. We only need to substitute the cross power spectral density $S_{\tilde{v}_i\tilde{v}_j}(\omega)$ in (38) with estimation results from Welch's method. Notice that we do not need to know the equilibrium velocity v^* in our data-driven method.

We remark that by choosing the periodogram as the spectral estimator, we recover the optimization framework in our previous work [23], where the energy-optimal controller parameters are selected by minimizing $\sum_{k=1}^{N-1}\omega_k^2\left|\tilde{V}(\omega_k)\right|^2$, equivalently to (41). The method presented in this paper gives solid theoretical justification to our previous framework and extends it to allow further improvement by choosing a better spectral estimator, e.g., Welch's method.

V. Numerical Results

In this section, we evaluate the optimization method proposed above using both synthetic data and real traffic data. With synthetic data, we have access to the underlying ground truth distribution of trajectories, which enables us to verify our theory. With real traffic data, we can show the potential of applying the proposed method in the real world. The evaluation scenarios include adaptive cruise control and connected cruise control with CHVs ahead of the CAT in the traffic. To showcase the potential of the proposed design to save energy with lean penetration of connectivity, we consider the scenario where the truck is only connected to a CHV L vehicles ahead.

A. Simulation Dataset

We consider two kinds of traffic data: driving in free-flow conditions and in traffic congestion [39]. These are shown in Fig. 2(a) and (b), respectively. In the second case, the leading vehicle frequently makes mild brakes, and the following vehicles have increasingly harsh brakes because of the string instability of human drivers [45], [46]. This string instability implies that the speed fluctuations of the vehicles in the distance may be milder than of those closer to the truck. With V2X connectivity, the CAT may respond not only to the immediate preceding vehicle but also the vehicles far in the distance. On the other hand, the observed phase-lags between the braking events motivate us to introduce the additional delays σ_i in (11). That is, it takes time for the behavior of preceding vehicles to affect the CAT, therefore, it shall "wait" before responding to vehicles far in the distance.

We generate synthetic speed trajectories for the preceding vehicles according to the stochastic modeling assumptions in Section III. In particular, we first generate the speed profile of vehicle L, and then simulate the following vehicles using a car-following model. According to Assumption 1 in Section III, the stochastic process $\tilde{v}_L(t)=v_L(t)-v^*$ is a mean zero differentiable Gaussian process. In this paper, we choose Matérn kernel [47]

$$R_{\tilde{v}_L\tilde{v}_L}(\tau)=C^2\frac{2^{1-\nu}}{\Gamma(\nu)}\left(\sqrt{2\nu}\frac{\tau}{\rho}\right)^{\nu}K_\nu\left(\sqrt{2\nu}\frac{\tau}{\rho}\right), \tag{42}$$

for this Gaussian process, where Γ is the Gamma function, K_ν is the modified Bessel function of the second kind, C, ρ and ν are positive parameters. In our simulations, we choose $v^*=25$ [m/s], $C=1$, $\rho=5$, and $\nu=\frac{5}{2}$. It can be proven that this process is second-order mean square differentiable [47].

To generate speed profiles for the following vehicles we use the optimal velocity model (OVM) for human driver behavior:

$$\begin{aligned}\dot{h}_i(t) &= v_{i+1}(t)-v_i(t)\\ \dot{v}_i(t) &= \alpha_{\mathrm{h}}(V(h_i(t-\sigma_{\mathrm{h}}))-v_i(t-\sigma_{\mathrm{h}}))\\ &\quad+\beta_{\mathrm{h}}(W(v_{i+1}(t-\sigma_{\mathrm{h}}))-v_i(t-\sigma_{\mathrm{h}})),\end{aligned} \tag{43}$$

for $i\in\{1,\dots,L-1\}$, where the range policy is given by

$$V_{\mathrm{h}}(h)=\max\left\{0,\min\{\kappa_{\mathrm{h}}(h-h_{\mathrm{st}}),v_{\max}\}\right\}, \tag{44}$$

and W is defined in (9). We choose parameters $\alpha_{\mathrm{h}}=0.2$ [1/s], $\beta_{\mathrm{h}}=0.8$ [1/s], $\kappa_{\mathrm{h}}=1.0$ [1/s], $\sigma_{\mathrm{h}}=1.0$ [s], and $L=8$. Fig. 2(c) shows the corresponding synthetic speed trajectories.

Remark. To keep the narrative simple, we show simulation results for the OVM only. However, we remark that our results are robust against the human driver behavior due to the data-driven nature of our approach. Apart from the OVM, we also conducted simulations on heterogeneous traffic where human driver models are randomly chosen as OVM or intelligent driver model [48], and we reached very similar conclusions to those with the OVM only.

B. Benefits of Connectivity

In this section, we compare the energy consumption for scenarios with and without connectivity in the traffic. Based on the synthetic dataset introduced in the previous section, we apply a *cross evaluation* method to evaluate the proposed controllers. This consists of two steps: observation and testing. In observation step, we observe the speed profile of the preceding

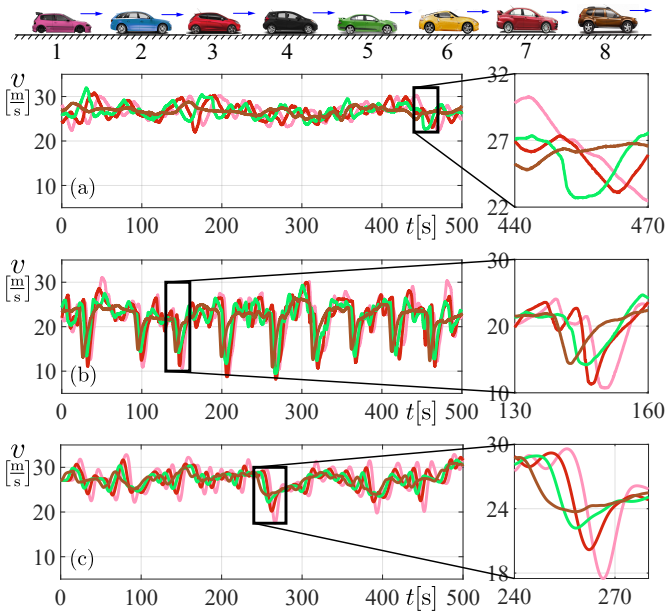

Fig. 2. Velocity profiles for vehicles 8 (brown), 5 (green), 3 (red), 1 (pink). (a) Experimental velocity data in free-flow traffic condition. (b) Experimental velocity data in congestion. (c) Synthetic data.

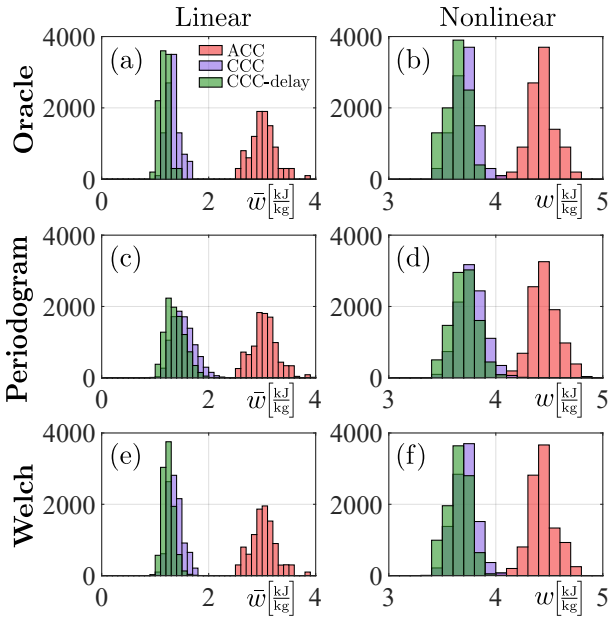

Fig. 3. Cross evaluation of energy consumption of ACC, CCC without additional delay and CCC with delay. In observation step, power spectral density is chosen from oracle knowledge (panels (a), (b)), periodogram estimator (panels (c), (d)) and Welch's method (panels (e), (f)), respectively.

vehicle, estimate the spectral density, and solve the optimization problem (38) to get the optimal controller parameters. In testing step, we simulate the truck for different preceding vehicle speed profiles, using the optimal parameters calculated in the observation step. The speed profile of the preceding vehicle in testing step shall have the same distribution as that in observation step. In particular, for the synthetic dataset, we create 101 candidate speed profiles for the preceding vehicle according to Section V-A and arbitrarily pick one for observation and another one for testing. Therefore, there are 101×100 observation-evaluation pairs.

Since the theoretical results are derived based on linearization, we conduct simulations for both linear and nonlinear systems. In the former case, we simulate the linearized system (13) where the nonlinear physical effects $f(v)$ and $\mathrm{sat}(\cdot)$ are dropped. Consequently the energy consumption model (27) is applied for evaluation. On the other hand, when simulating the nonlinear system (1,6,11), we take into account all nonlinear effects, and use (18) to calculate the energy consumption.

When there is no connected vehicle in the traffic, the truck can only collect information about the motion of the vehicle immediately ahead. We refer to this as adaptive cruise control (ACC). The corresponding energy consumption will serve as a benchmark, and will be compared to the CCC controllers which exploit V2X connectivity. The acceleration command of adaptive cruise control is given by (7). Thus, (14,15,16) yields

$$V(s) = T(s)V_1(s), \quad T(s) = \frac{\beta_1 s + \alpha\kappa}{s^2 e^{s\sigma} + (\alpha+\beta_1)s + \alpha\kappa}. \tag{45}$$

Fig. 3 shows the cross evaluation result for the energy consumption of adaptive cruise control (ACC), connected cruise control without additional information delay (CCC), and

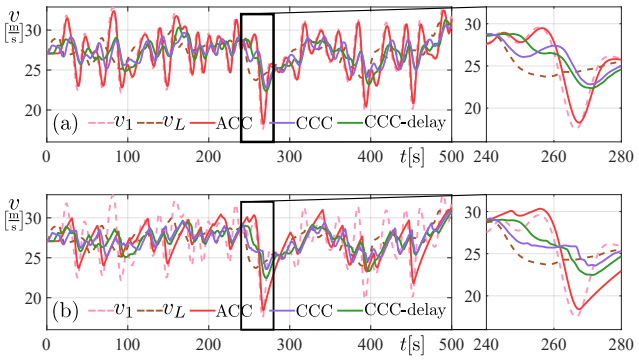

Fig. 4. Speed profile of the CAT following synthetic trajectory in Fig. 2(c) using ACC, CCC and CCC with additional delay. We choose vehicle 8 as leading vehicle ($L = 8$). Spectral densities are chosen from oracle knowledge. (a) Linear simulation. (b) Nonlinear simulation.

	ACC [kJ/kg]	CCC [kJ/kg]	CCC-Delay [kJ/kg]
Oracle	3.018	1.331 (−55.89%)	1.178 (−60.98%)
Periodogram	3.044	1.529 (−49.77%)	1.378 (−54.72%)
Welch	3.020	1.379 (−54.35%)	1.244 (−58.80%)

TABLE I
AVERAGE ENERGY CONSUMPTION $\bar{w}$ IN LINEAR SIMULATION.

	ACC [kJ/kg]	CCC [kJ/kg]	CCC-Delay [kJ/kg]
Oracle	4.438	3.709 (−16.44%)	3.635 (−18.11%)
Periodogram	4.453	3.771 (−15.33%)	3.705 (−16.82%)
Welch	4.436	3.712 (−16.34%)	3.653 (−17.66%)

TABLE II
AVERAGE ENERGY CONSUMPTION w IN NONLINEAR SIMULATION.

CCC with delay (CCC-Delay). In the observation step, power spectral density can be chosen from oracle knowledge (panels (a) and (b)), periodogram estimator (panels (c) and (d)) and Welch's method (panels (e) and (f)), respectively. For both estimators, information from V2X connectivity can bring significant energy reduction compared to ACC, where no V2X connectivity is available. The average energy consumption is compared for the different cases in Tables I and II. In the linear case (Table I), connectivity can reduce the energy consumption by around 50%, while in the nonlinear case, at least 15% energy is saved. Note that these savings are achieved by adding a single connected vehicle in the traffic flow. The additional delay leads to additional 5% energy saving in the linear case, and additional 2% saving in the nonlinear case.

Although the energy reduction rate is considerably larger for the linear case than for the nonlinear case, it is significant even for nonlinear dynamics. This shows that our method is robust to the occurrence of nonlinear physical effects. We also note that the 15% energy benefit thanks to V2X connectivity is obtained in scenarios with heavy traffic congestion, which are the most energy-sensitive scenarios. In daily driving, connectivity (using controllers different from ours) was reported to bring around 3% energy benefits [49].

To further investigate how connectivity and the additional delay benefits the energy consumption, in Fig. 4 we plot the speed profiles of the CAT executing ACC, CCC, and CCC with additional delay, respectively. We choose synthetic speed trajectories shown in Fig. 2(c) for preceding vehicles, and vehicle 8 is the leading vehicle ($L = 8$). Simulation results of the linearized system and the nonlinear system are shown in panels (a) and (b) of Fig. 4, respectively. The ACC controller closely follows the trajectory of its immediate predecessor. As highlighted by the zoom-ins, there is heavy braking around $t = 260$ [s], which results in heavy braking with ACC. Thus, ACC consumes significant energy. However, with connectivity the CAT has access to the states of preceding vehicles in the distance. Hence the truck knows that the leading vehicle L brakes around $t = 240$ [s], and using CCC it can brake in advance, creating enough safe margin to avoid heavy braking at $t = 260$ [s]. Moreover, since the braking behavior takes around 10 seconds to propagate from vehicle L to 1, the truck does not need to react immediately to the brake. Instead, it can purposely delay the reaction with a few seconds. Thus, CCC with additional delay further reduces the speed perturbation.

C. Choice of Spectral Estimator

In this section, we show that choosing better spectral estimator can help us get closer to the energy-optimal parameters and reduce the energy consumption. There is a fundamental trade-off between the variance and frequency resolution for spectral estimators [42]. Welch's method has less variance than periodogram, at the cost of lower frequency resolution. We compare these two spectral estimators by simulations using the synthetic data described in Section V-A.

Figure 5 illustrates the performance of the spectral estimators. Panel (a) shows the mean of the sample autocorrelation function, which is in excellent agreement with the oracle

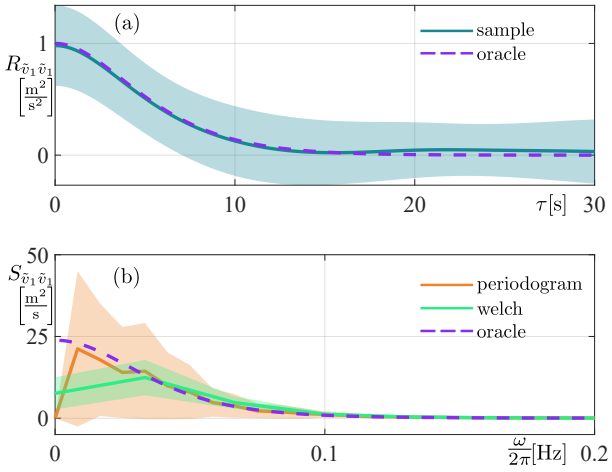

Fig. 5. Comparison of the periodogram and Welch's spectral estimators. (a) Sample-based correlation function and the oracle correlation function (42). (b) Spectral estimations and the oracle power spectral density. Solid curves denote the mean while the standard deviation is indicated by shading.

(42). Panel (b) compares the power spectral density calculated by the periodogram (orange curve and shading) and Welch's method (green curve and shading) with the oracle power spectral density (purple dashed curve). The latter is obtained as the Fourier transform of (42). The means of spectral estimators match the oracle very well except at zero frequency. Note that the spectral density at zero frequency does not influence the objective function in (38). The periodogram estimator has higher resolution compared to Welch's method, but the variance is significantly higher. In practice, Welch's method demands more data but, when stationary assumptions hold for a long enough time, this method can bring more precise spectral description.

Fig. 6 compares the controller parameters chosen from oracle, periodogram and Welch's method, denoted as $\theta^{(\text{o})}$, $\theta^{(\text{p})}$, and $\theta^{(\text{w})}$ respectively, where $\theta \in \{\beta_1, \beta_L, \sigma_L\}$. One may observe that Welch's method achieves better concentration around the oracle parameters than the periodogram, and the resulting parameters lie closer to the oracle which is the optimum based on ground truth distribution.

Finally, we compare the energy consumption of the linearized and nonlinear dynamics using parameters chosen from oracle, periodogram and Welch's method. In the linear case, the energy consumption is evaluated using surrogate model (27) which neglects the nonlinear physical effects. We denote the corresponding energy consumptions as $\bar{w}^{(\text{o})}$, $\bar{w}^{(\text{p})}$ and $\bar{w}^{(\text{w})}$. In the nonlinear case, the energy consumption is evaluated using (18), and the corresponding energy consumptions are $w^{(\text{o})}$, $w^{(\text{p})}$ and $w^{(\text{w})}$. To compare the three spectral estimations, we compute the relative energy advantages

$$\Delta\bar{w}^{(\diamondsuit\square)} = (\bar{w}^{(\diamondsuit)} - \bar{w}^{(\square)})/\bar{w}^{(\square)} \,, \tag{46a}$$

$$\Delta w^{(\diamondsuit\square)} = (w^{(\diamondsuit)} - w^{(\square)})/w^{(\square)} \,, \tag{46b}$$

where $\diamondsuit, \square \in \{\text{o}, \text{p}, \text{w}\}$. The histograms of 10100 observation-testing pairs are shown in Fig. 7. The panels in the left column show linear results, while in the right column we show nonlinear results. In panels (a) and (b), we compare the

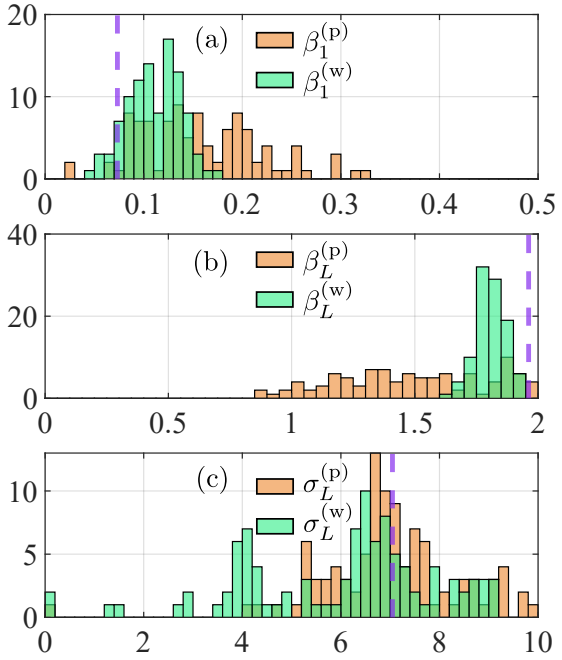

Fig. 6. Distribution of controller parameters optimized for energy consumption. The orange histogram corresponds to the periodogram estimator while green corresponds to Welch's method. Purple dashed lines correspond to the optimal controller parameters chosen with oracle knowledge of speed distribution.

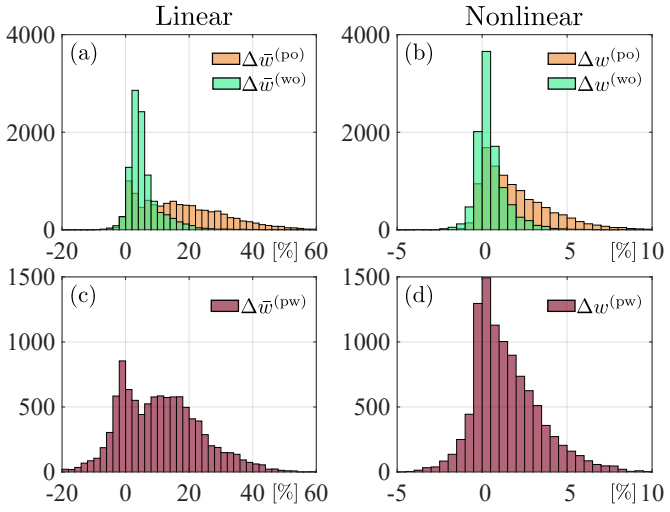

Fig. 7. Comparison of energy consumption of the periodogram and Welch's estimator. (a), (b) Energy consumption compared to the oracle. (c), (d) Direct comparison of the two spectral estimators.

energy consumptions of the estimators to those of the oracle. The distribution of energy consumption is more concentrated around 0 for Welch's method, which means in most cases, the parameter given by Welch's method can achieve similar energy consumption as the benchmark oracle parameter. We also compare these two spectral estimators directly in panels (c) and (d). For most of the cases, Welch's method consumes less energy than periodogram as $\Delta\bar{w}^{(\mathrm{pw})}$ and $\Delta w^{(\mathrm{pw})}$is distributed more towards positive values. On average, the periodogram parameters consume 10.78% more energy than Welch parameters in linear case while 1.42% more energy in nonlinear case.

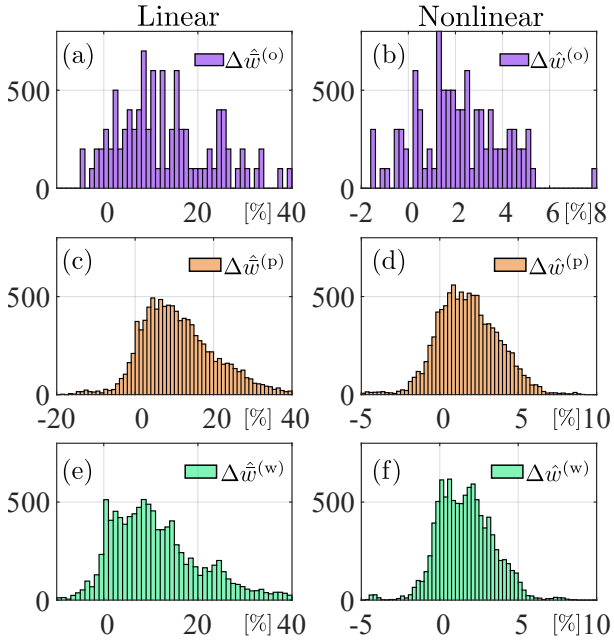

Fig. 8. Comparison of controllers with and without additional delay. The histograms are distributed towards positive values in each panel, which indicates that the additional delay leads to energy savings.

D. Benefits of Additional Delay

Here we quantify the benefits of incorporating the additional delays σ_i into the controller (11). Recall that these delays were introduced based on the following intuition. Considering lean penetration of connected vehicles, the CAT may connect to vehicles far in the distance. Introducing additional delays enables the CAT to "wait" until the effect of the distant vehicles' motion propagate closer, and thus, it may achieve a more energy-efficient response. In this section, we compare the controller with and without additional delay using synthetic data as well as experimental data.

First, we apply the proposed method to find the optimal parameters for the case when $\sigma_i = 0$. The corresponding energy consumption values using oracle, periodogram and Welch's method are denoted by $\hat{w}^{(\mathrm{o})}$, $\hat{w}^{(\mathrm{p})}$ and $\hat{w}^{(\mathrm{w})}$, respectively. In order to compare this controller with the one with additional time delay, we define the relative energy advantages

$$\Delta\hat{\bar{w}}^{(\Diamond)} = (\hat{\bar{w}}^{(\Diamond)} - \bar{w}^{(\Diamond)})/\bar{w}^{(\Diamond)} , \tag{47a}$$

$$\Delta\hat{w}^{(\Diamond)} = (\hat{w}^{(\Diamond)} - w^{(\Diamond)})/w^{(\Diamond)} , \tag{47b}$$

for linear and nonlinear cases, respectively, where $\Diamond \in \{\mathrm{o}, \mathrm{p}, \mathrm{w}\}$, cf. (46). The corresponding histograms are shown in Fig. 8. For all methods used, the additional delay brings energy benefits. In the linear case, oracle, periodogram and Welch's method save 11.53%, 9.86% and 9.77% energy on average. In the nonlinear case, the average energy benefits are 2.00%, 1.76% and 1.59%, respectively. Although the nonlinearity in the dynamics impairs the advantage, the difference is still significant.

For lean penetration of connectivity, the number of vehicles driving between the CAT and the leading CHV may be varying. In previous simulations, we fixed the leading vehicle to

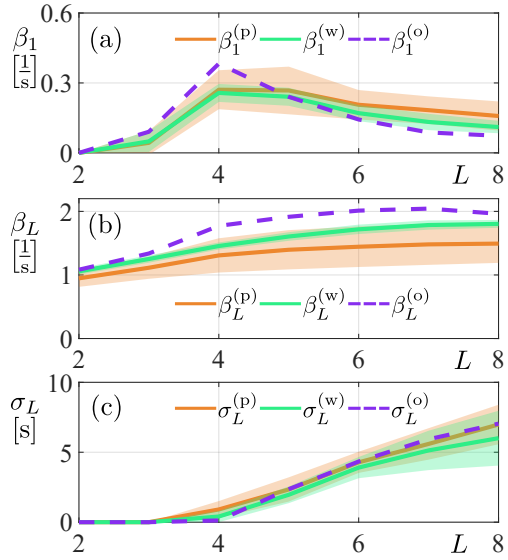

Fig. 9. Controller parameters for varying leader ($L = 2, \ldots, 8$ vehicles ahead of the CAT). Each synthetic dataset produces a controller parameter triplet $(\beta_1, \beta_L, \sigma_L)$. The means of parameters optimized with periodogram and Welch's method are plotted with solid line. The widths of shaded areas are determined by the standard deviations. Controller parameters from oracle knowledge of spectral density are plotted with dashed lines.

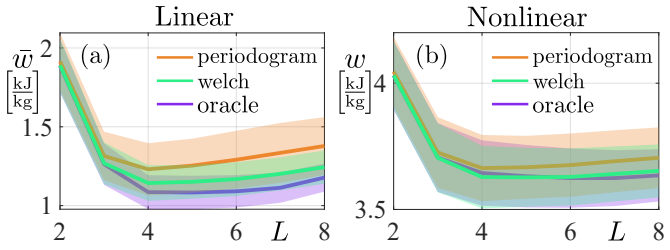

Fig. 10. Energy consumption for varying leader ($L = 2, \cdots, 8$) using 10100 observation-evaluation pairs. Solid lines represent the mean values while the widths of shaded areas indicate the standard deviations.

$L = 8$. Now, we investigate optimal controller parameters and the corresponding energy consumption for different leading vehicles $L = 2, \ldots, 8$ and show that our method is agnostic to the change of leading vehicle.

In Fig. 9, we show optimized controller parameters for different leading vehicles. For each of the 101 synthetic datasets, spectral densities are estimated with periodogram and Welch's method resulting in 101 controller parameter sets $(\beta_1^{(\diamondsuit)}, \beta_L^{(\diamondsuit)}, \sigma_L^{(\diamondsuit)}), \diamondsuit \in \{\mathrm{p}, \mathrm{w}\}$. The mean of the parameters are plotted with solid line, and the widths of the shaded areas indicate standard deviation. Since the datasets are synthetic, we have access to the oracle knowledge of spectral density. The correspondingly optimized oracle parameters are plotted with dashed line. The mean periodogram and Welch parameters are close to the oracle parameters, and the Welch parameters have smaller deviation for β_1 and β_L. Also note that when L is small ($L = 2, 3, 4$) the optimal delay is $\sigma_L = 0$ [s]. This can be explained intuitively: when the leading vehicle L is close to the ego vehicle, instantaneous response is preferred without additional waiting time [23].

The energy consumption results with respect to periodogram, Welch and oracle parameters are plotted in Fig. 10.

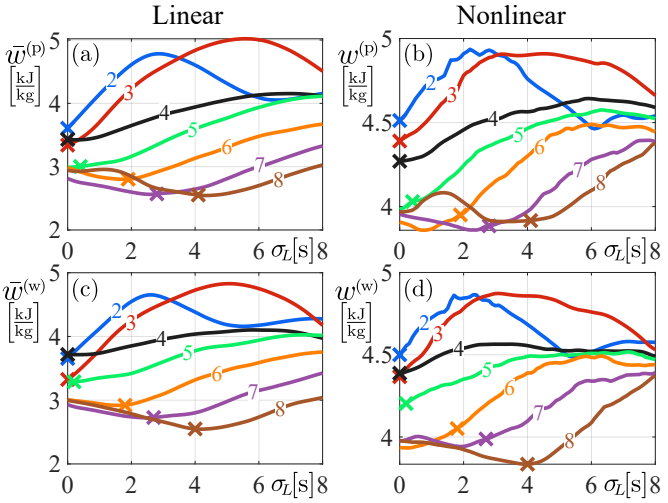

Fig. 11. Energy consumption as a function of the additional delay σ_L in the controller for different leading vehicles ($L = 2, \ldots, 8$), for the case of a real traffic congestion dataset. Crosses correspond to the optimal σ_L values based on periodogram and Welch's method. Panels (a) and (c) show the energy consumptions for the linear case, while panels (b) and (d) correspond to the nonlinear case.

The means of energy consumption are plotted with solid line and the standard deviation determines the width of shaded areas. In linear case, shown in panel (a), oracle parameters consume lower average energy than periodogram and Welch parameters, while in nonlinear case depicted in panel (b), Welch parameters have similar and sometimes better average performance as oracle parameters. In both cases, Welch parameters have lower average energy consumption than periodogram parameters. In addition, connecting to vehicles farther in the distance saves more energy than connecting to vehicles nearby due to the string instability of human-driven vehicles ahead. In other words, vehicles in the distance may have lower speed variations, which provides smoother reference trajectories for the controller.

We make a further case study on the experimental traffic congestion data shown in Fig. 2(b). We show the optimal energy consumption as a function of the leading vehicle's index L and the additional delay σ_L. For each fixed value of σ_L, we optimize for β and β_L using periodogram and Welch's method. The corresponding energy consumptions are plotted in Fig. 11, and the optimal delays σ_L chosen by periodogram and Welch's method are marked with crosses. When the CAT is connected to vehicles nearby, for example $L = 2, 3, 4, 5$, the additional delay does not bring extra energy benefits, since the propagation time of the congestion waves between vehicle L and the CAT is short. However, for more distant connections, such as $L = 6, 7, 8$, incorporating the additional delay σ_{L} yields significant energy savings. This is consistent with results in Fig. 9(c). Furthermore, connecting to vehicles farther in the distance leads to more energy benefits than connecting to vehicles nearby, which is consistent with Fig. 10.

VI. Conclusion

In this paper, we designed longitudinal controllers for a connected automated truck traveling in mixed traffic that con-

sists of connected and non-connected vehicles. We leveraged that the truck has access to beyond-line-of-sight information via vehicle-to-vehicle communication, and we introduced an additional delay in the control law when responding to distant connected vehicles. Human-driven traffic was modeled by stationary stochastic processes and car-following models, where the spectral properties of the stochastic processes were linked to the average energy consumption with a new theorem. The controllers were optimized by minimizing average energy consumption. In the underlying optimization problem, the spectral density of the stochastic process was estimated from data using spectral estimators. We showed that our optimization framework can select designs with significant energy saving. It can also facilitate improvements when utilizing motion information from distant vehicles. Simulations with large amount of synthetic data showed that energy benefits can be realized even with lean penetration of connected vehicles, regardless of their positions in the traffic. Further investigations about how the energy consumption is affected by the penetration rate of connected vehicles are left for future research.

The theory in this paper is based on linear systems under stationarity assumptions. It can be readily applied not only to trucks but other types of vehicles independent of their propulsion system. Although nonlinearities were not considered in the parameter optimization, the simulations of the nonlinear dynamics showed the robustness of our method. We remark that energy optimization and evaluation were done in an offline fashion in this paper. Controller parameters were optimized using training datasets and kept constant during testing simulations. Furthermore, our spectral method focuses on the average performance in steady state and transient responses are omitted. To implement controllers with online optimization in dynamically changing traffic environments, transients in the traffic conditions should be considered and the wide-sense stationarity assumption needs to be relaxed. Our future research will also focus on addressing nonlinearities and online energy optimization.

REFERENCES

[1] T. Ard, L. Guo, R. A. Dollar, A. Fayazi, N. Goulet, Y. Jia, B. Ayalew, and A. Vahidi, "Energy and flow effects of optimal automated driving in mixed traffic: Vehicle-in-the-loop experimental results," *Transportation Research Part C*, vol. 130, p. 103168, 2021.

[2] C. R. He, H. Maurer, and G. Orosz, "Fuel consumption optimization of heavy-duty vehicles with grade, wind, and traffic information," *Journal of Computational and Nonlinear Dynamics*, vol. 11, no. 6, 2016.

[3] C. R. He, A. Alan, T. G. Molnár, S. S. Avedisov, A. H. Bell, R. Zukouski, M. Hunkler, J. Yan, and G. Orosz, "Improving fuel economy of heavy-duty vehicles in daily driving," in *American Control Conference (ACC)*. IEEE, 2020, pp. 2306–2311.

[4] G. Guo and Q. Wang, "Fuel-efficient en route speed planning and tracking control of truck platoons," *IEEE Transactions on Intelligent Transportation Systems*, vol. 20, no. 8, pp. 3091–3103, 2019.

[5] "Taxonomy and definitions for terms related to cooperative driving automation for on-road motor vehicles," SAE International, Warrendale, PA, Standard, May 2020.

[6] V. Turri, B. Besselink, and K. H. Johansson, "Cooperative look-ahead control for fuel-efficient and safe heavy-duty vehicle platooning," *IEEE Transactions on Control Systems Technology*, vol. 25, no. 1, pp. 12–28, 2017.

[7] S. E. Li, Y. Zheng, K. Li, Y. Wu, J. K. Hedrick, F. Gao, and H. Zhang, "Dynamical modeling and distributed control of connected and automated vehicles: Challenges and opportunities," *IEEE Intelligent Transportation Systems Magazine*, vol. 9, no. 3, pp. 46–58, 2017.

[8] L. Bertoni, J. Guanetti, M. Basso, M. Masoero, S. Cetinkunt, and F. Borrelli, "An adaptive cruise control for connected energy-saving electric vehicles," *IFAC-PapersOnLine*, vol. 50, no. 1, pp. 2359–2364, 2017, 20th IFAC World Congress.

[9] B. McAuliffe, M. Lammert, X.-Y. Lu, S. Shladover, M.-D. Surcel, and A. Kailas, "Influences on energy savings of heavy trucks using cooperative adaptive cruise control," in *WCX World Congress Experience*. SAE International, 2018.

[10] Z. Wang, G. Wu, and M. J. Barth, "A review on cooperative adaptive cruise control (CACC) systems: Architectures, controls, and applications," in *21st IEEE Intelligent Transportation Systems Conference (ITSC)*, 2018, pp. 2884–2891.

[11] E. van Nunen, J. Reinders, E. Semsar-Kazerooni, and N. van de Wouw, "String stable model predictive cooperative adaptive cruise control for heterogeneous platoons," *IEEE Transactions on Intelligent Vehicles*, vol. 4, no. 2, pp. 186–196, 2019.

[12] G. Guo, D. Yang, and R. Zhang, "Distributed trajectory optimization and platooning of vehicles to guarantee smooth traffic flow," *IEEE Transactions on Intelligent Vehicles*, pp. 1–1, 2022.

[13] A. Vahidi and A. Sciarretta, "Energy saving potentials of connected and automated vehicles," *Transportation Research Part C*, vol. 95, pp. 822–843, 2018.

[14] Z. Yao, Y. Wang, B. Liu, B. Zhao, and Y. Jiang, "Fuel consumption and transportation emissions evaluation of mixed traffic flow with connected automated vehicles and human-driven vehicles on expressway," *Energy*, vol. 230, p. 120766, 2021.

[15] T. Ard, R. A. Dollar, A. Vahidi, Y. Zhang, and D. Karbowski, "Microsimulation of energy and flow effects from optimal automated driving in mixed traffic," *Transportation Research Part C*, vol. 120, p. 102806, 2020.

[16] Y. Zhang and C. G. Cassandras, "An impact study of integrating connected automated vehicles with conventional traffic," *Annual Reviews in Control*, vol. 48, pp. 347–356, 2019.

[17] L. Zhao, A. Malikopoulos, and J. Rios-Torres, "Optimal control of connected and automated vehicles at roundabouts: An investigation in a mixed-traffic environment," *IFAC-PapersOnLine*, vol. 51, no. 9, pp. 73–78, 2018.

[18] X. Fang, H. Li, T. Tettamanti, A. Eichberger, and M. Fellendorf, "Effects of automated vehicle models at the mixed traffic situation on a motorway scenario," *Energies*, vol. 15, no. 6, p. 2008, 2022.

[19] S. S. Avedisov, G. Bansal, and G. Orosz, "Impacts of connected automated vehicles on freeway traffic patterns at different penetration levels," *IEEE Transactions on Intelligent Transportation Systems*, vol. 23, no. 5, pp. 4305–4318, 2022.

[20] G. Orosz, "Connected cruise control: modelling, delay effects, and nonlinear behaviour," *Vehicle System Dynamics*, vol. 54, no. 8, pp. 1147–1176, 2016.

[21] C. Huang, R. Salehi, T. Ersal, and A. G. Stefanopoulou, "An energy and emission conscious adaptive cruise controller for a connected automated diesel truck," *Vehicle System Dynamics*, vol. 58, no. 5, pp. 805–825, 2020.

[22] S. V. D. Hoef, J. Mårtensson, D. V. Dimarogonas, and K. H. Johansson, "A predictive framework for dynamic heavy-duty vehicle platoon coordination," *ACM Transactions on Cyber-Physical Systems*, vol. 4, no. 1, 2019.

[23] C. R. He, J. I. Ge, and G. Orosz, "Fuel efficient connected cruise control for heavy-duty trucks in real traffic," *IEEE Transactions on Control Systems Technology*, vol. 28, no. 6, pp. 2474–2481, 2020.

[24] G. Orosz, J. I. Ge, C. R. He, S. S. Avedisov, W. B. Qin, and L. Zhang, "Seeing beyond the line of site – controlling connected automated vehicles," *ASME Mechanical Engineering Magazine*, vol. 139, no. 12, pp. S8–S12, 2017.

[25] M. Shen, T. G. Molnár, C. R. He, A. H. Bell, M. Hunkler, D. Oppermann, R. Zukouski, J. Yan, and G. Orosz, "Saving energy with delayed information in connected vehicle systems," in *2021 American Control Conference (ACC)*. IEEE, 2021, pp. 1625–1630.

[26] M. Shen, C. R. He, A. H. Bell, and G. Orosz, "Energy-efficient stochastic connected cruise control," in *24th IEEE Intelligent Transportation Systems Conference (ITSC)*, 2021, pp. 2082–2088.

[27] M. Bando, K. Hasebe, A. Nakayama, A. Shibata, and Y. Sugiyama, "Dynamical model of traffic congestion and numerical simulation," *Physical Review E*, vol. 51, pp. 1035–1042, Feb 1995.

[28] M. Bando, K. Hasebe, K. Nakanishi, and A. Nakayama, "Analysis of optimal velocity model with explicit delay," *Physical Review E*, vol. 58, no. 5, p. 5429, 1998.

[29] T. Ersal, I. Kolmanovsky, N. Masoud, N. Ozay, J. Scruggs, R. Vasudevan, and G. Orosz, "Connected and automated road vehicles: state of the art and future challenges," *Vehicle System Dynamics*, vol. 58, no. 5, pp. 672–704, 2020.

[30] G. Guo, P. Li, and L.-Y. Hao, "A new quadratic spacing policy and adaptive fault-tolerant platooning with actuator saturation," *IEEE Transactions on Intelligent Transportation Systems*, vol. 23, no. 2, pp. 1200–1212, 2022.

[31] L. Zhang and G. Orosz, "Motif-based design for connected vehicle systems in presence of heterogeneous connectivity structures and time delays," *IEEE Transactions on Intelligent Transportation Systems*, vol. 17, no. 6, pp. 1638–1651, 2016.

[32] S. Wong, L. Jiang, R. Walters, T. G. Molnár, G. Orosz, and R. Yu, "Traffic forecasting using vehicle-to-vehicle communication," in *3rd Conference on Learning for Dynamics and Control*, vol. 144. PMLR, 2021, pp. 917–929.

[33] T. G. Molnár, D. Upadhyay, M. Hopka, M. Van Nieuwstadt, and G. Orosz, "Delayed Lagrangian continuum models for on-board traffic prediction," *Transportation Research Part C*, vol. 123, p. 102991, 2021.

[34] M. J. Lighthill and G. B. Whitham, "On kinematic waves II. A theory of traffic flow on long crowded roads," *Proceedings of the Royal Society of London A*, vol. 229, no. 1178, pp. 317–345, 1955.

[35] G. F. Newell, "A simplified car-following theory: a lower order model," *Transportation Research Part B*, vol. 36, no. 3, pp. 195–205, 2002.

[36] A. Sciarretta, G. De Nunzio, and L. L. Ojeda, "Optimal ecodriving control: Energy-efficient driving of road vehicles as an optimal control problem," *IEEE Control Systems Magazine*, vol. 35, no. 5, pp. 71–90, 2015.

[37] A. Sciarretta and A. Vahidi, *Energy-Efficient Driving of Road Vehicles*. Springer, 2020.

[38] B. Hajek, *Random Processes for Engineers*. Cambridge University Press, 2015.

[39] J. I. Ge, S. S. Avedisov, C. R. He, W. B. Qin, M. Sadeghpour, and G. Orosz, "Experimental validation of connected automated vehicle design among human-driven vehicles," *Transportation Research Part C*, vol. 91, pp. 335–352, 2018.

[40] R. V. Roy and P. D. Spanos, "Power spectral density of nonlinear system response: The recursion method," *Journal of Applied Mechanics*, vol. 60, no. 2, pp. 358–365, 06 1993.

[41] P. Wu, Y. Zhao, and X. Xu, "Power spectral density analysis for nonlinear systems based on volterra series," *Applied Mathematics and Mechanics*, vol. 42, no. 12, pp. 1743–1758, 2021.

[42] R. H. Shumway and D. S. Stoffer, *Time Series Analysis and Its Applications*. Springer, 2017.

[43] P. Welch, "The use of fast Fourier transform for the estimation of power spectra: A method based on time averaging over short, modified periodograms," *IEEE Transactions on Audio and Electroacoustics*, vol. 15, no. 2, pp. 70–73, 1967.

[44] MathWorks, Inc., *fmincon*, Natick, MA, USA, 2022. [Online]. Available: https://www.mathworks.com/help/optim/ug/fmincon.html

[45] S. Feng, Y. Zhang, S. E. Li, Z. Cao, H. X. Liu, and L. Li, "String stability for vehicular platoon control: Definitions and analysis methods," *Annual Reviews in Control*, vol. 47, pp. 81–97, 2019.

[46] J. Ploeg, N. van de Wouw, and H. Nijmeijer, "$\mathcal{L}_p$ string stability of cascaded systems: Application to vehicle platooning," *IEEE Transactions on Control Systems Technology*, vol. 22, no. 2, pp. 786–793, 2014.

[47] C. Rasmussen and C. Williams, *Gaussian Processes for Machine Learning*. MIT Press, 2006.

[48] A. Kesting, M. Treiber, and D. Helbing, "Enhanced intelligent driver model to access the impact of driving strategies on traffic capacity," *Philosophical Transactions of the Royal Society A*, vol. 368, no. 1928, pp. 4585–4605, 2010.

[49] "Tusimple environmental, social, and governance report," TuSimple Holdings, Inc., Tech. Rep., 2021.

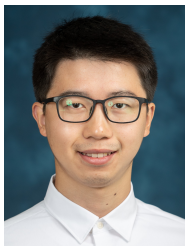

Minghao Shen received the BSc degree in Automotive Engineering from Jilin University in 2019. He is currently working towards PhD degree in Mechanical Engineering at the University of Michigan, Ann Arbor. His research interests include stochastic process, control theory, machine learning, and their applications in planning and control of connected and automated vehicles.

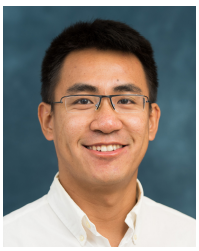

Chaozhe R. He received the BSc degree in Applied Mathematics from the Beijing University of Aeronautics and Astronautics in 2012, the MSc and PhD in Mechanical Engineering from the University of Michigan, Ann Arbor, USA, in 2015 and 2018 respectively. Dr. He is with Plus.ai Inc. and is working on planning and control algorithm development. His research interests include dynamics and control of connected automated vehicles, optimal and nonlinear control theory, and data-driven control.

Tamas G. Molnar received his BSc degree in Mechatronics Engineering, MSc and PhD degrees in Mechanical Engineering from the Budapest University of Technology and Economics, Hungary, in 2013, 2015 and 2018. He held postdoctoral position at the University of Michigan, Ann Arbor between 2018 and 2020. Since 2020 he is a postdoctoral fellow at the California Institute of Technology, Pasadena. His research interests include nonlinear dynamics and control, safety-critical control, and time delay systems with applications to connected automated vehicles, robotic systems, and machine tool vibrations.

A. Harvey Bell received his bachelor degree from the University of Michigan, Ann Arbor. He pursued graduate studies at the University of Pennsylvania and the University of Michigan, Dearborn. He is currently a Charles S and Ann S Hutchins Professor of Practice in Engineering at the University of Michigan, Ann Arbor where he also serves as the Co-director of the Multidisciplinary Design Program. He spent his 39-year long career in the automotive industry with General Motors where some of his significant achievements were: Chief Engineering a 2.5 Liter Engine, Vehicle Chief Engineering the 4th Generation Camaro and Firebird, Executive Director of the Advanced Vehicle Development Center for North America.

Gábor Orosz received the MSc degree in Engineering Physics from the Budapest University of Technology, Hungary, in 2002 and the PhD degree in Engineering Mathematics from the University of Bristol, UK, in 2006. He held postdoctoral positions at the University of Exeter, UK, and at the University of California, Santa Barbara. In 2010, he joined the University of Michigan, Ann Arbor where he is currently an Associate Professor in Mechanical Engineering and in Civil and Environmental Engineering. His research interests include nonlinear dynamics and control, time delay systems, and machine learning with applications to connected and automated vehicles, traffic flow, and biological networks.